BNL-224932-2023-JAAM

GRP-COCAFP-4

Bimetallic-Derived Catalytic Structures for CO2-Assisted Ethane Activation

Z. Xie

To be published in "Accounts of Chemical Research"

August 2023

Chemistry Department

Brookhaven National Laboratory

U.S. Department of Energy

USDOE Office of Science (SC), Basic Energy Sciences (BES) (SC-22)

Notice: This manuscript has been authored by employees of Brookhaven Science Associates, LLC under Contract No.DE-SC0012704 with the U.S. Department of Energy. The publisher by accepting the manuscript for publication acknowledges that the United States Government retains a non-exclusive, paid-up, irrevocable, world-wide license to publish or reproduce the published form of this manuscript, or allow others to do so, for United States Government purposes.

DISCLAIMER

This report was prepared as an account of work sponsored by an agency of the United States Government. Neither the United States Government nor any agency thereof, nor any of their employees, nor any of their contractors, subcontractors, or their employees, makes any warranty, express or implied, or assumes any legal liability or responsibility for the accuracy, completeness, or any third party's use or the results of such use of any information, apparatus, product, or process disclosed, or represents that its use would not infringe privately owned rights. Reference herein to any specific commercial product, process, or service by trade name, trademark, manufacturer, or otherwise, does not necessarily constitute or imply its endorsement, recommendation, or favoring by the United States Government or any agency thereof or its contractors or subcontractors. The views and opinions of authors expressed herein do not necessarily state or reflect those of the United States Government or any agency thereof.

Bimetallic-derived catalytic structures for CO_2-assisted ethane activation

Zhenhua Xie,[1,2] *Jingguang. G. Chen*[1,2*]

[1] Chemistry Division, Brookhaven National Laboratory, Upton, NY 11973, USA

[2] Department of Chemical Engineering, Columbia University, New York, NY 10027, USA

CONSPECTUS:

In recent years, the simultaneous upgrading of CO_2 and ethane has emerged as a promising approach for generating valuable gaseous (CO, H_2 and ethylene) and liquid (aromatics and C3 oxygenates) chemicals from the greenhouse gas CO_2 and large-reserved shale gas. The key challenges for controlling product selectivity lie in the selective C–H/C–C bond cleavage of ethane with the assistance of CO_2. Bimetallic-derived catalysts likely undergo alloying or oxygen-induced segregation under reaction conditions, thus providing diverse types of interfacial sites, e.g., metal/support (M/M'O_x) interface and metal oxide/metal (M'O_x/M) inverse interface, that are beneficial for selective CO_2-assisted ethane upgrading. The alloying extent can be initially predicted by cohesive energy and atomic radius (or Wigner-Seitz radius), while the preference for segregation to form the on-top suboxide can be approximated using work function, electronegativity, and binding strength of adsorbed oxygen. Furthermore, bimetallic-derived catalysts are typically supported on high surface area oxides. Modifying the reducibility and acidity/basicity of the oxide supports and introducing surface defects facilitate CO_2 activation and oxygen supplies for ethane activation. Using in situ synchrotron characterization and density functional theory (DFT) calculations, we found that the electronic properties of oxygen species influence the selective cleavage of C–H/C–C bonds in ethane, with electron-deficient oxygen over the metal (or alloy) surface promoting non-selective bond scission to produce syngas and electron-enriched oxygen over the metal oxide/metal interface enhancing selective C–H scission to yield ethylene. We further demonstrate that the preferred structures of the catalyst surfaces, either alloy surfaces or metal oxide/metal inverse interfaces, can be controlled through the appropriate choice of metal combinations and their atomic ratios. Through a comprehensive comparison of experimental results and DFT calculations, the selectivity of C−C/C−H bond scission is correlated

with the thermodynamically favorable bimetallic-derived structures (i.e., alloy surfaces or metal oxide/metal inverse interfaces) under reaction conditions over a wide range of bimetallic catalysts. These findings not only offer structural and mechanistic insights into bimetallic-derived catalysts, but also provide design principles of selective catalysts for CO_2-assisted activation of ethane and other light alkanes. The Accounts concludes by discussing challenges and opportunities in designing advanced bimetallic-derived catalysts, incorporating new reaction chemistries for other products, employing precise synthesis strategies for well-defined structures with optimized site densities, and leveraging time/spatial/energy-resolved in situ spectroscopy/scattering/microscopy techniques for comprehensive structural analysis. The research methodologies established here are helpful for the investigation of dynamic alloy and interfacial structures and should inspire more efforts for the simultaneous upgrading of CO_2 and shale gas.

KEY REFERENCES:

- Porosoff, M. D.; Myint, M. N. Z.; Kattel, S.; Xie, Z.; Gomez, E.; Liu, P.; Chen, J. G. Identifying Different Types of Catalysts for CO_2 Reduction by Ethane through Dry Reforming and Oxidative Dehydrogenation. *Angew. Chem. Int. Ed.* 2015, 54 (51), 15501–15505.[1] This study demonstrated the selective upgrading of ethane and CO_2 into either ethylene by the oxidative dehydrogenation pathway or syngas (CO and H_2) by the dry reforming pathway.
- Yan, B.; Yao, S.; Kattel, S.; Wu, Q.; Xie, Z.; Gomez, E.; Liu, P.; Su, D.; Chen, J. G. Active Sites for Tandem Reactions of CO_2 Reduction and Ethane Dehydrogenation. *Proc. Natl. Acad. Sci. U.S.A.* 2018, 115 (33), 8278–8283.[2] This study identified two types of interfacial structures enabling the selective ethane activation with CO_2. It also highlighted the

possibility of controlling the synthesis of these distinct active sites, thereby influencing product selectivity, by adjusting the metal ratios.

- Xie, Z.; Tian, D.; Xie, M.; Yang, S.-Z.; Xu, Y.; Rui, N.; Lee, J. H.; Senanayake, S. D.; Li, K.; Wang, H.; Kattel, S.; Chen, J. G. Interfacial Active Sites for CO_2 Assisted Selective Cleavage of C–C/C–H Bonds in Ethane. *Chem* 2020, 6 (10), 2703–2716.[3] This work established a comprehensive methodology to unravel the complex bimetallic-derived interfacial structures and revealed their pivotal roles in dictating the availability of oxygen species with distinct electronic properties for the selective bond activation of ethane.
- Xie, Z.; Wang, X.; Chen, X.; Liu, P.; Chen, J. G. General Descriptors for CO_2-Assisted Selective C–H/C–C Bond Scission in Ethane. *J. Am. Chem. Soc.* 2022, 144 (9), 4186–4195.[4] Two key factors were uncovered to determine the reaction-induced metal alloy or metal oxide/metal interfacial configurations that control the selective C─H/C─C bond scission in CO_2-assisted ethane conversion to either ethylene or syngas.

1. INTRODUCTION

The rapid rise in CO_2 emissions has resulted in significant concerns regarding global climate crisis and ocean acidification.[5,6] Various mitigation strategies have been proposed, including CO_2 capture[7,8] and catalytic conversion[9–12], among which thermocatalytic CO_2 hydrogenation and electrocatalytic CO_2 reduction have shown promise in producing a diverse range of valuable chemicals. However, large-scale implementation depends on the availability of CO_2-free hydrogen and renewable energy. The abundance of ethane in shale gas, as an alternative hydrogen and carbon source, presents opportunities for catalytic conversion of CO_2. Ethane is often underutilized in conventional petrochemical processes, despite its substantial global supply from shale gas reserves.[13] Recent developments have explored the simultaneous upgrading of ethane and CO_2, enabling the synthesis of valuable gaseous (CO, H_2 and olefins) and liquid (e.g., aromatics and oxygenates) chemicals that are essential to various industries worldwide.[14–16] A recent analysis of CO_2 footprint reveals the potential to achieve a net CO_2 reduction in the CO_2-ethane reactions.[17]

To achieve efficient CO_2-ethane upgrading, the key challenge is activating CO_2 and selectively cleaving the C–C bond (dry reforming: $C_2H_6+CO_2 \rightarrow 4CO+3H_2$) and C–H bond (oxidative dehydrogenation: $C_2H_6+CO_2 \rightarrow C_2H_4+CO+H_2O$) of ethane.[1,3] Bimetallic-derived catalysts show promise due to the ligand, strain, ensemble, and interfacial effects.[18] These catalysts exhibit unique electronic, chemical, and steric properties, both in alloy structures and at interfacial sites like metal/support and metal oxide/metal interfaces. However, controlling and identifying the active sites responsible for specific reaction pathways is challenging due to the presence of multiple active sites and their dynamic response to synthesis and reaction conditions. Thus, understanding the structure-function relationships of bimetallic-derived catalysts is crucial. Precise atomic-level

synthesis and comprehensive in situ characterization techniques are essential for guiding the design of bimetallic-derived catalysts for simultaneous CO_2 and ethane upgrading.

Here, we present our research efforts focused on understanding and advancing bimetallic-derived catalytic structures for selective CO_2-assisted activation of ethane. We firstly discuss the multiple interactions occurring on bimetallic catalysts, the underlying principles, and the reaction complexity of the CO_2-ethane reaction. By utilizing composition effects, enhanced oxidation-induced segregation effects, and strong alloying effects, we demonstrate how the desired catalytic structures can be controlled to selectively cleave C–H/C–C bonds. Through comprehensive in situ characterization and theoretical examinations, we identify general descriptors that dictate the preference for forming alloy or metal oxide/metal interfacial structures under reaction conditions, which in turn control the product selectivity. Finally, we discuss challenges, opportunities, and potential applications of bimetallic-derived catalysts in the simultaneous upgrading of CO_2 and light alkanes.

2. MULTIPLE INTERACTIONS IN BIMETALLIC-DERIVED CATALYSTS

The structure and catalytic performance of bimetallic catalysts are profoundly influenced by synthesis methods, pretreatment conditions, and reaction atmosphere. Various synthesis methods like impregnation, co-precipitation, sol-gel, atomic layer deposition, and hydrothermal synthesis offer different levels of control over the initial distribution of the two metals.[19] Co-precipitation, for instance, often results in a more uniform metal distribution, whereas impregnation may cause metal segregation. Moreover, reduction temperature during preparation thermodynamically and kinetically affects alloy phase transitions and metal-support interactions. The pretreatment atmosphere, such as reduction (e.g., H_2 or CO) or oxidation (e.g., O_2 or steam), can further induce surface alloy formation, metal segregation, or surface reconstruction. Additionally, under reaction

conditions with oxygen species such as those from CO_2 activation, one metal component may undergo oxidation, introducing interfacial structures and interactions. Typically, bimetallic-derived catalysts on high surface area supports exhibit five primary types of interactions: metal-metal, metal-support, metal-adsorbate, support-adsorbate, and interface-adsorbate. An appropriate combination of the distinct structures can endow a catalyst with multiple functionalities for the CO_2-alkane reactions. It is crucial to understand the underlying principles governing these interactions to design desired catalysts that possess coordinated active sites by enhancing specific interactions.

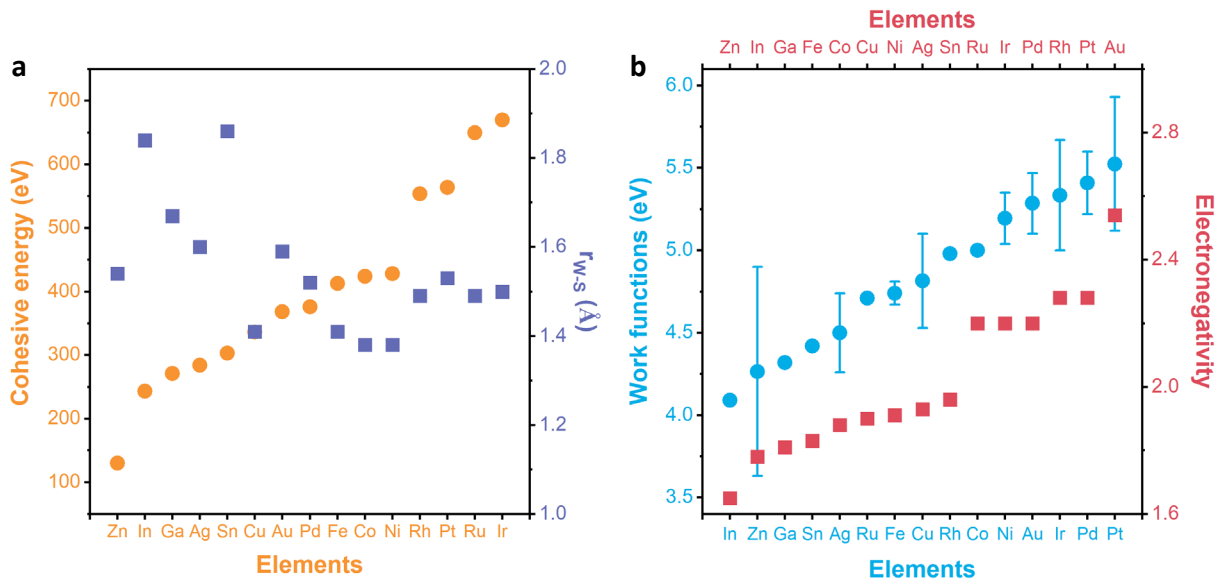

Figure 1. Key factors of late transition and p-block metal elements. (a) Cohesive energy and Wigner-Seitz radius. (b) Work functions and electronegativity. Data were collected from refs. 20–22.

2.1. Metal-metal interaction

Subject to the minimization of total free energy ($\Delta G_{M\text{-}M'}$), the metal-metal interaction within bimetallic nanoparticles/clusters tends to adopt various thermodynamically favorable configurations, including random (disordered or mixed), ordered (intermetallic compounds), core@shell, or Janus structures.[14,19] The resulting configuration is determined by factors such as relative cohesive energy, atomic radius (or Wigner-Seitz radius, $r_{W\text{-}S}$), particle size, surface energy and facets, elemental compositions, and temperature range. Generally, when the cohesive energy and atomic radii (Figure 1a) of the two metal elements (M and M') are similar, random alloy structures are usually favored. Yet, achieving an ordered or intermetallic structure can be challenging due to the stringent thermodynamic (e.g., stronger M-M' bonding) and kinetic (e.g., matched concentrations, favorable temperature range, and sufficient growth time) requirements.[23] Unless specified, the term "alloy" is used to denote the random structure rather than the intermetallic structure.

Furthermore, surface segregation is a commonly observed phenomenon in bimetallic nanoparticles/clusters, leading to the formation of core@shell and Janus structures, particularly when there is a significant difference in relative cohesive energy (>20%) and relative Wigner-Seitz radius (>4%) between the constituent elements.[24] In such cases, the element with lower cohesive energy and larger atomic radius tends to segregate towards the surface.[25] The composition and size of the nanoparticles/clusters can further influence the extent and nature of surface segregation. As the particle size decreases from the bulk to the nanoscale, the surface energy increases due to the higher surface-to-volume ratio, favoring the segregation of the element with lower surface energy towards the surface. Moreover, smaller nanoparticles/clusters enable faster diffusion rates due to

shorter diffusion distances and higher atomic mobility, allowing a facile transport of atoms towards or away from the surface.

2.2. Metal-support interaction

A catalyst support serves not only as a carrier for metal dispersion but also often imposes electronic and geometric perturbations on the metal ensembles it supports. The interaction between the metal and the support is primarily governed by factors such as the work function, reducibility of the support, atom mobility, and lattice compatibility. Subject to the energy alignment of the Fermi levels between the metal and support of different work functions, electron transfers or surface band bending occur within the first few layers of the contact, often resulting in unique physical and chemical properties at the interface.[26] Depending on the proportion of the contact perimeter or atoms, the so-called interfacial effect can play a significant role as the metal particle size decreases to nanoscale (e.g., < 4 nm).[27] The strength of the metal-support interaction impacts the stability, chemical composition, particle configuration, and surface termination of the bimetallic ensembles. Supports with vacancies in cations or oxygen (such as reducible metal oxides) or silanol groups (such as silica) on their surfaces can strongly anchor the metal ensembles, making them resistant to thermal sintering. However, the preference of the support to strongly bind one of the elements in the bimetallic ensembles can cause alloy segregation, either towards the surface or into the support lattice.

Usually, the lattice mismatch between the metal and the oxide support can modify the lateral positions of the interfacial atoms in the metal. Because oxides are generally much stiffer than metals, the “mismatch strains" primarily occur in the metal ensemble with lattice expansion or compression, particularly near the interface.[28] The interfacial strain can lower the barrier for vacancy formation in the reducible oxide, such as CeO_2 and TiO_2. Furthermore, under reducing or

vacuum conditions, the reduced MO_x moiety (e.g., TiO_x, CeO_x, and NbO_x) with higher mobility likely migrates toward the metal surface to minimize the high surface energy of the metal nanoparticles/clusters.[29] This migration can lead to a partial or complete encapsulation of the metal ensembles by amorphous or crystallized support suboxide species, leading to the so-called strong metal-support interaction (SMSI). In general, the metal-support interaction offers additional possibilities for controlling the physical and chemical properties of the supported metal ensembles, while also providing interfacial sites that can enhance catalytic performance.

2.3. Bimetallic-adsorbate, support-adsorbate, and interface-adsorbate interactions

The thermodynamically stable structure under pretreatment and reaction conditions is influenced both by the metal-metal and metal-support interactions and by the interactions of the metal, support, and interface with adsorbates. Under the CO_2-ethane reactions, bimetallic catalysts are subject to both reductive and oxidative potentials imposed by the reactants, intermediates, and products, which may induce additional changes in the catalyst structures.

Beyond ethane activation, metal sites may also activate CO_2, primarily following the formate or carboxylate pathways.[30,31] Yet, because adsorbed oxygen is present from CO_2 dissociation, surface segregation may occur when the metal-oxygen bonding is strong enough to overcome the metal-metal bonding within the bimetallic ensemble.[32] Thus, metal oxophilicity is a descriptor that can be employed to approximate or predict the segregation trend for a given bimetallic ensemble. Generally, as shown in Figure 1b, metals with low electronegativity,[33] low work function,[34] and/or high d-band center relative to the Fermi level[32] tend to bind oxygen species stronger, leading to the segregation of the specific metal to form an O*-adsorbed surface or oxide on the surface of the bimetallic ensemble, often referred to as the metal oxide-metal ($M'O_x$/M) inverse interface[35,36].

Most oxide supports, except for a few early transition metal oxides (e.g., Cr_2O_3, Nb_2O_5, and V_2O_5), generally exhibit lower activity in alkane activation compared to metal surfaces, while they play a crucial role in CO_2 activation. Both redox sites and acid/base centers can contribute to the CO_2 reduction pathway. Metal ions (Lewis acid) and oxygen ions/surface hydroxyls (Lewis base) in metal oxide supports can act as the active sites for the adsorption and activation of CO_2 via (bi)carbonate intermediates due to surface acidity/basicity.[30,31] Base metal oxides (e.g., MgO and La_2O_3) are often used as promoters or supports to improve catalyst basicity for enhanced CO_2 adsorption and coke resistance. Furthermore, reducible supports (e.g., CeO_2) with redox properties can generate oxygen vacancies to enhance CO_2 activation, especially when combined with supported metal ensembles.[37–39] Additionally, the proximity of metal and metal oxide provides dual active sites for preferential reactant activation and facilitates the transport of intermediates between the metal and support (e.g., hydrogen spillover) or vice versa (e.g., oxygen spillover), which can modify the CO_2-ethane reaction.[39,40]

3. BIMETALLIC-DERIVED CATALYSTS FOR CO_2-ETHANE REACTION

3.1 General reaction mechanisms of CO_2-assisted ethane activation

The control of the extent of dry reforming of ethane (DRE) and CO_2-assisted oxidative dehydrogenation of ethane (CO_2-ODHE) contributions is crucial for selectively upgrading ethane and CO_2 into gaseous and liquid products. Figure 2a illustrates the key intermediates and potential reaction pathways for DRE and CO_2-ODHE, as well as other potential reactions including direct dehydrogenation of ethane (DHE), reverse water gas-shift (RWGS), and hydrogenolysis. Designing a catalyst with targeted properties poses significant challenges as it involves improving five crucial reaction steps: CO_2 activation, oxygen transfer and supply, activation of C–H/C–C/C=C bonds, carbon scavenge via the C=O bond formation, and desorption of C_2H_4 and

CO.[39,41,42,15,14,43] Balancing these processes is essential to achieve high activity, selectivity, and stability.[14]

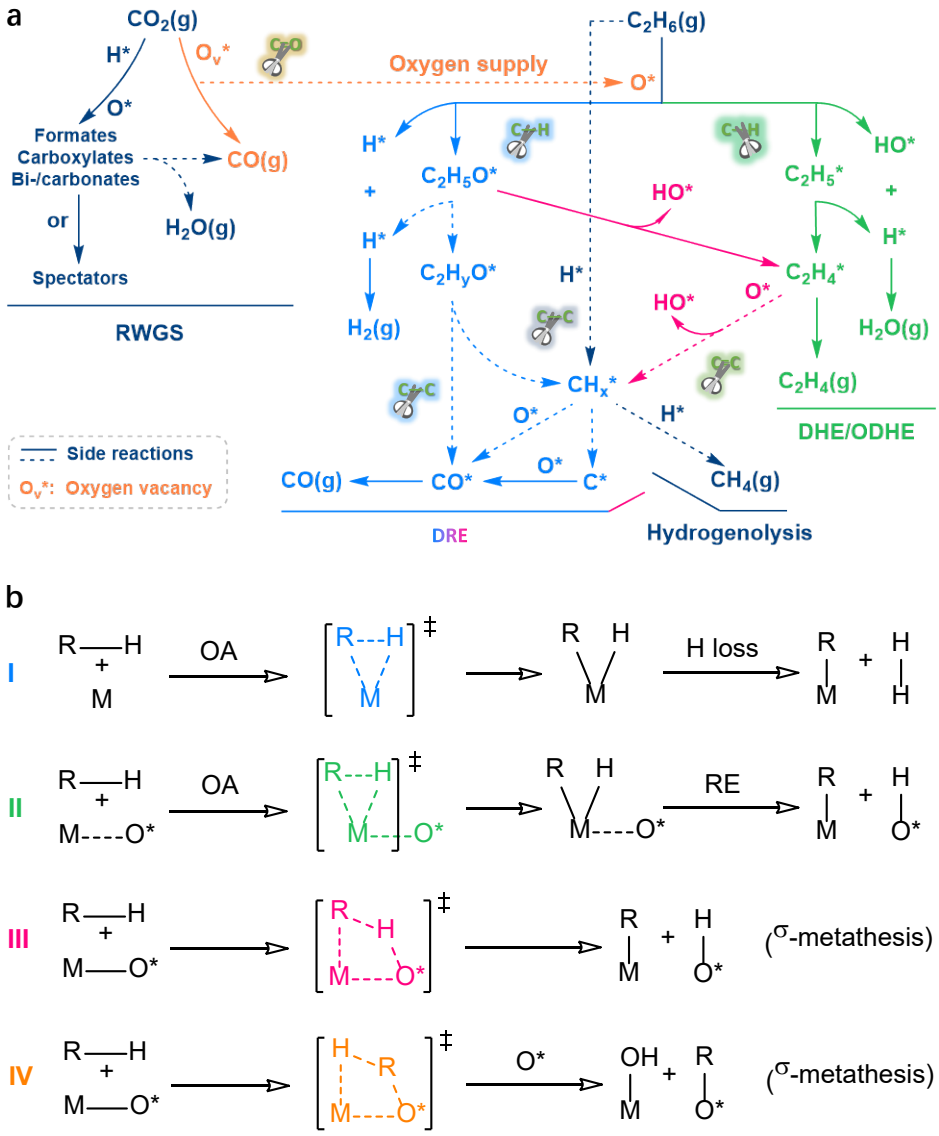

Figure 2. Mechanistic insights into the CO_2-ethane reaction. (a) Schematic illustration of potential reaction network. Adapted with permission from ref. 14. Copyright 2021, Elsevier. (b) Summary of the typical modes of C–H bond activation of alkane in heterogeneous catalysis. OA and RE refer to oxidative addition and reductive elimination, respectively.

It remains challenging to control the selective scission of C–H/C–C bonds in alkanes. Analogous to organometallic chemistry, C–H bond activation in alkanes typically proceeds with electrophilic (or radical) activation, oxidative addition (OA) or σ-bond metathesis (σ-MT) mechanism with the latter two being more common in heterogeneous catalysis.[44–46] As shown in Figure 2b, in a two-step OA mode (I), a metal atom or a low-valence metal ion (d^n, $n\neq0$) inserts into the C–H bond to form a three-center transition state (TS) complex, followed by a subsequent elimination of hydride as H_2 (e.g., direct dehydrogenation) to somewhat compensate the energy penalty from the C–H bond dissociation. In the presence of oxidants like CO_2, oxygen adatoms/ions (O*) or site-pair of metal (ion) and vicinal O* (M-O*) may become surface-prevailing. The extent of oxygen's participation in the transition state leads to the classification of CO_2-assisted C–H bond activation into the indirect mechanism via a two-step OA mode (II) and the direct mechanism via a one-step σ-MT mode (III or IV). The indirect mode initiates C–H bond activation via oxidative addition, involving either metal atoms (e.g., Pt-based catalysts)[43,47] or low-valence metal ions (e.g., $Cr^{\delta+}$, $Mo^{\delta+}$, $V^{\delta+}$, and $Co^{\delta+}$)[41,42,48] inserting into the C–H bond to form a three-center TS complex, followed by H* elimination by CO_2-derived O*. Alternatively, the CO_2-derived O* species can directly participate in C–H bond activation in the transition state, forming a four-center TS complex, followed by the formation of metastable alkanepoxy species or energetically more favorable species (e.g., OH or H_2O). In comparison, the direct C–C bond activation in the first step is more difficult due to the kinetic (sterically less accessible, highly directional, and statistically less abundant) and thermodynamic (typically more endothermic due to the two relatively weak M-C bonds) hindrances; instead, the C–C/C=C bonds in the intermediates (such as C_2H_y* or C_2H_yO* from ethane) after the initial C–H bond activation likely become facile to be cleaved with the appearance of an accessible π feature (as a σ donor and π acceptor) in the frontier orbitals, to which

a strong backdonation from the M-O* sites may occur. Therefore, a delicate design of the chemical properties of the M-O* sites is pivotal to achieve the selective bond cleavage and in turn the desirable product selectivity from the CO_2-ethane reactions.

3.2. Compositional effect in tuning bimetallic-derived structures

We investigated the compositional effect on thermodynamically favorable bimetallic configurations in CO_2-ethane reactions using CeO_2-supported Ni_xFe_y catalysts. Both Ni and Fe have similar ε_{coh} (428 vs 413 kJ/mol)[22] and $r_{W\text{-}S}$ (1.38 vs 1.41 Å)[22], indicating the potential formation of a random or mixed alloy structure at an equal molar ratio. Yet, Fe has a lower work function (4.74 vs 5.20 eV)[20] as well as lower electronegativity (1.83 vs 1.91)[19], representing a higher oxophilicity than Ni.

Figure 3 shows that as the Ni/Fe ratios varied from 3:0 to 3:1, 1:3, and 0:3, a synergistic effect between Fe and Ni was identified to tune the ethane conversion and C_2H_4/CO selectivity compared to the monometallic catalysts. Moreover, 90% CO selectivity was observed over the Ni_3Fe_1/CeO_2 catalyst in contrast to the 78% C_2H_4 selectivity over the Ni_1Fe_3/CeO_2 catalyst. The in situ X-ray diffraction (XRD) measurements revealed the partial reduction of Ce^{4+} in CeO_2 to Ce^{3+} and the formation of a Ni-rich NiFe alloy with an fcc structure on both catalysts during H_2 reduction. The in situ X-ray absorption (XAS) measurements validated the metallic state of Ni over both catalysts, while the Fe species retained a similar near-edge feature between Fe(II)O and $Fe(II, III)_3O_4$. The extended X-ray absorption fine structure (EXAFS) analysis approximated the NiFe alloy particle size of 2.5-4.0 nm. Thus, the additional Fe species, particularly in Ni_1Fe_3/CeO_2, are expected to reside on the metal (or alloy) surface and/or the CeO_2 support, as verified by scanning transmission electron microscopy (STEM) with annular dark-field (ADF) imaging and electron energy loss spectroscopy (EELS) analysis. The EELS line scan profiles of Fe showed the existence of an

amorphous FeO_x layer (~2 nm) in Ni_1Fe_3/CeO_2, which was absent in Ni_3Fe_1/CeO_2. The control Fe_3/CeO_2 catalyst with the predominant FeO_x/CeO_2 interaction was nearly inactive. Hence, the combined in situ/ex situ characterization unraveled two types of representative active structures, i.e., Ni(Fe)/CeO_x interface over Ni_3Fe_1/CeO_2 and FeO_x/Ni(Fe) inverse interface over Ni_1Fe_3/CeO_2 under CO_2-ethane reaction conditions.

Density functional theory (DFT) calculations indicated that the FeO_x/Ni(111) interface promoted the stability of *CH_3CH_2 for the dehydrogenation pathway to C_2H_4.[2] In contrast, the formation of *CH_3CH_2O and its subsequent dehydrogenation and C–C bond cleavage reactions via *CH_3CO were favored over the alloy (Ni/bulk-terminated-Ni_3Fe(111)) and metal (Ni(111)) surfaces, thus leading to the reforming pathway to produce CO and H_2. Overall, these results highlight the potential for controlling the selective bond cleavage in the CO_2-ethane reactions by carefully selecting the combination of metal elements and varying their compositions to form either metallic alloys or FeO_x/Ni inverse interfaces.

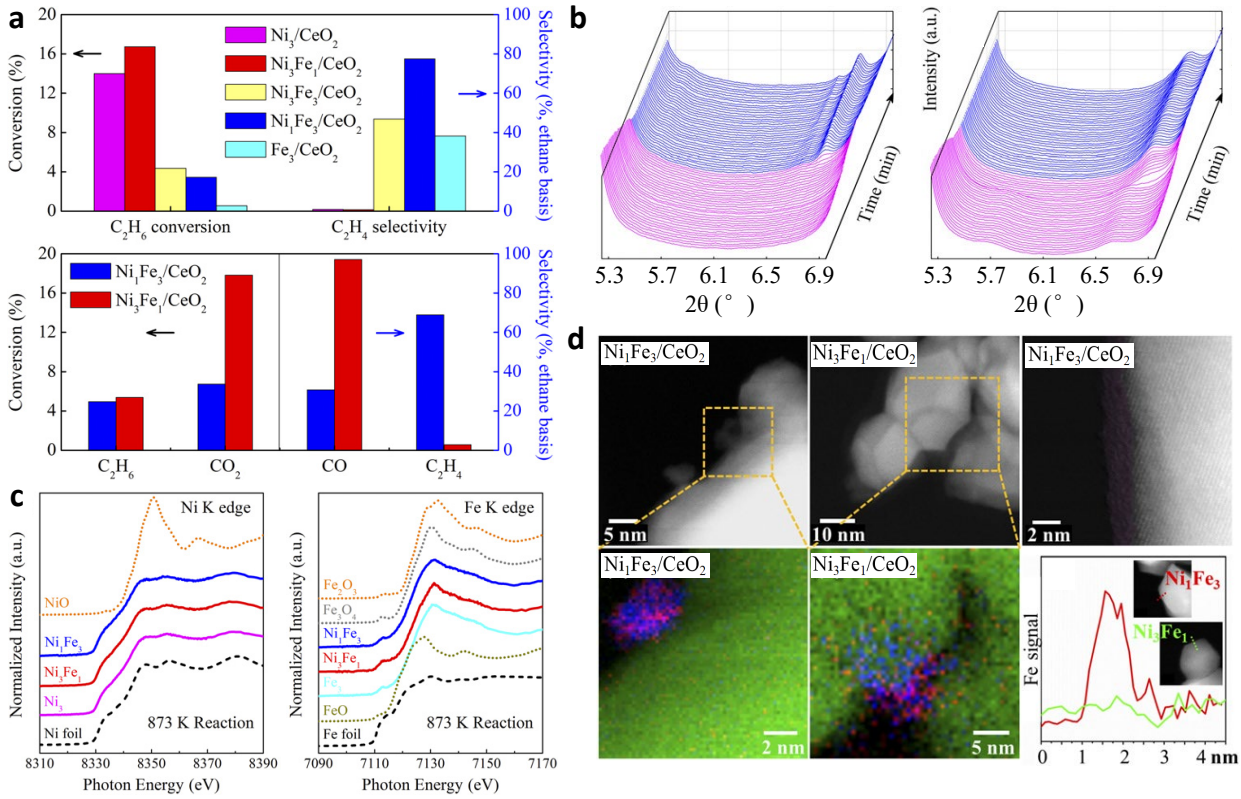

Figure 3. Composition effect of Fe/Ni over the selective CO_2-ethane upgrading. (a) Results for the CO_2-ethane reaction over Ni_xFe_y/CeO_2 catalysts using a flow reactor. (b) In situ XRD profiles under the CO_2-ethane stream. (c) XANES spectra of Ni and Fe K-edges under reaction conditions as well as referential standards. (d) Annular dark-field STEM images and EELS analysis. Color in mappings: Ce, green; Ni, blue; Fe, red. Adapted with permission from ref. 2. Copyright 2018, National Academy of Sciences.

3.3. Enhanced segregation effect in creating metal oxide/metal inverse interfaces

To enhance the formation of a favorable metal oxide/metal inverse interface during the CO_2-ethane reactions, one can opt for a bimetallic combination that promotes segregation of the oxophilic element toward the surface for facile oxidation to form suboxides. Alternatively, selecting metals with a significant difference in oxophilicity can help overcome alloy bonding in the presence of oxygen species, despite that alloy structures may be favored under reduction conditions. The $PdFe/CeO_2$[3] and $PdIn/CeO_2$[4] catalysts were used as examples to illustrate the effectiveness of these strategies in promoting the formation of the inverse interfaces.

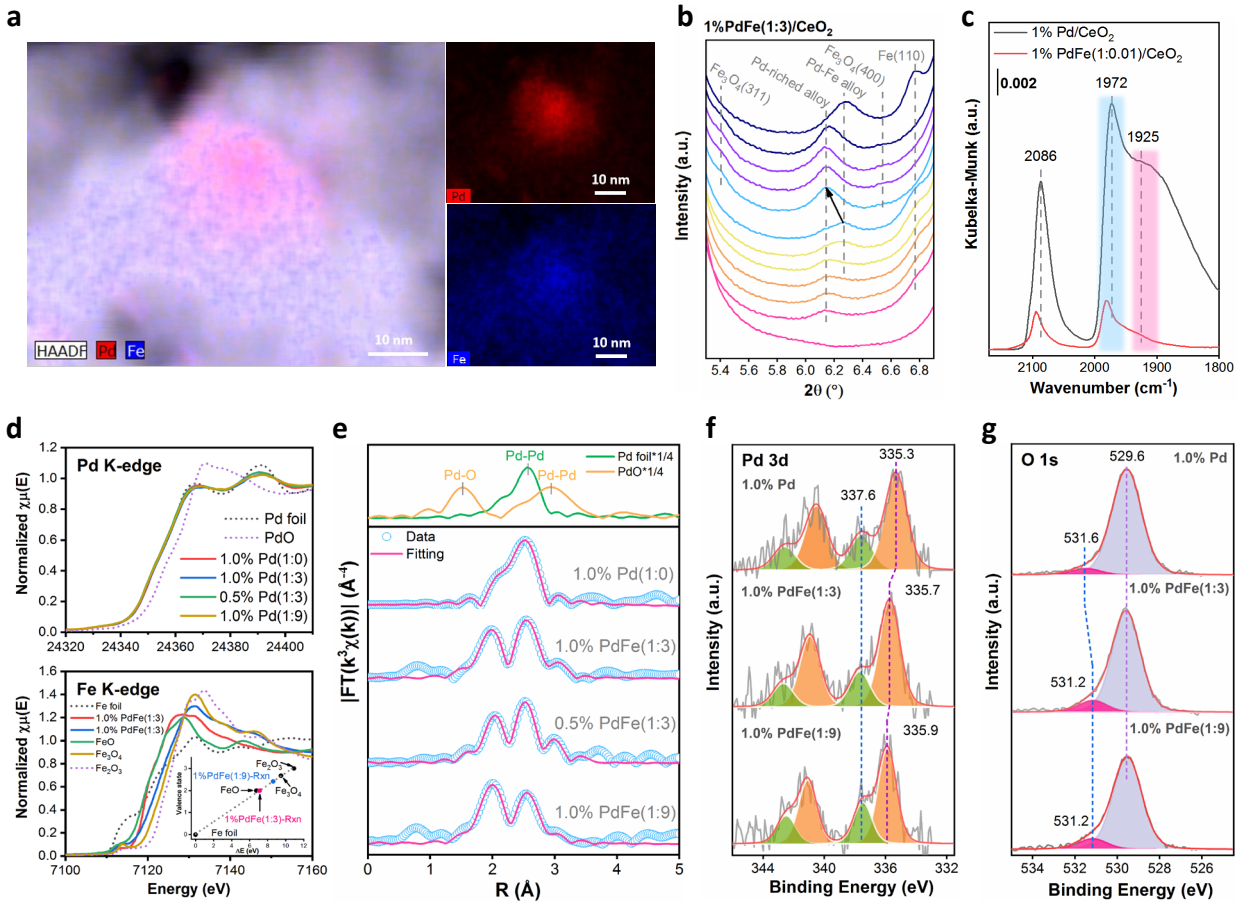

Figure 4. In situ structural characterization of bimetallic-derived metal oxide/metal inverse interface. (a) HAADF-STEM image and EDS mappings over the spent $PdFe_3/CeO_2$ catalyst. (b)

In situ XRD patterns on $PdFe_3/CeO_2$ under different conditions. (c) DRIFT spectra of adsorbed CO over different catalysts at room temperature. (d) and (e) In situ XANES spectra of Pd K-edge and Fe K-edge of different catalysts under reaction conditions. (e) In situ Fourier transformed EXAFS spectra of Pd K-edge of different catalysts under reaction conditions. (f) and (g) AP-XPS spectra of Pd 3d (f) and O 1s (g) of different catalysts under reaction conditions. Adapted with permission from ref. 3. Copyright 2020, Elsevier.

Pd shows a weaker ε_{coh} (376 vs 413 kJ/mol) and a larger $r_{W\text{-}S}$ (1.52 vs 1.41 Å) than Fe, suggesting that Pd prefers to reside on the surface. However, Fe is much more oxophilic than Pd as indicated by the difference in their work functions (4.74 vs 5.41 eV) and electronegativity (1.83 vs 2.20), posing an enhanced potential of oxidation-induced segregation of Fe to the surface than that in the NiFe system. The in situ XRD (Figure 4) revealed the formation of PdFe alloys after the H_2-reduction treatment, which somewhat de-alloyed with the appearance of a weak Fe_3O_4 diffraction peak after the exposure to the CO_2-ethane stream. The in situ XAS measurements validated the formation of Pd-Fe bonds and detected an interfacial Pd-(O)-Fe bonds under reaction conditions. The diffuse reflectance infrared Fourier transform spectroscopy (DRIFTS) of CO chemisorption revealed the surface decoration of Pd ensembles by FeO_x species. Ambient-pressure X-ray photoelectron spectroscopy (AP-XPS) detected charge transfer from Pd to the oxygen species due to the presence of the FeO_x/Pd interface as confirmed in the HAADF-EDS imaging. The combined characterization results indicated an oxidation-induced effect that caused Fe to segregate onto Pd nanoparticles during the reaction, resulting in the FeO_x/Pd interface. Together with DFT calculations (Figure 5), the electronic features of oxygen species within distinct interfaces were identified to be strongly correlated with the selective C–H/C–C bond cleavage of ethane[3]: the electron-enriched oxygen at the FeO_x/Pd interface enhances the C–H bond scission to yield C_2H_4;

the electron-deficient oxygen species derived from the Pd/CeO_x interface of the control Pd/CeO_2 catalyst boosts the non-selective bond scission to produce syngas; the FeO_x/CeO_2 interface is not a primary active site for reactants activation, but it mediates oxygen supply and confines metal ensembles. This study provides insights into the roles of oxygen species at distinct interfacial sites in controlling the selective bond cleavage of ethane.

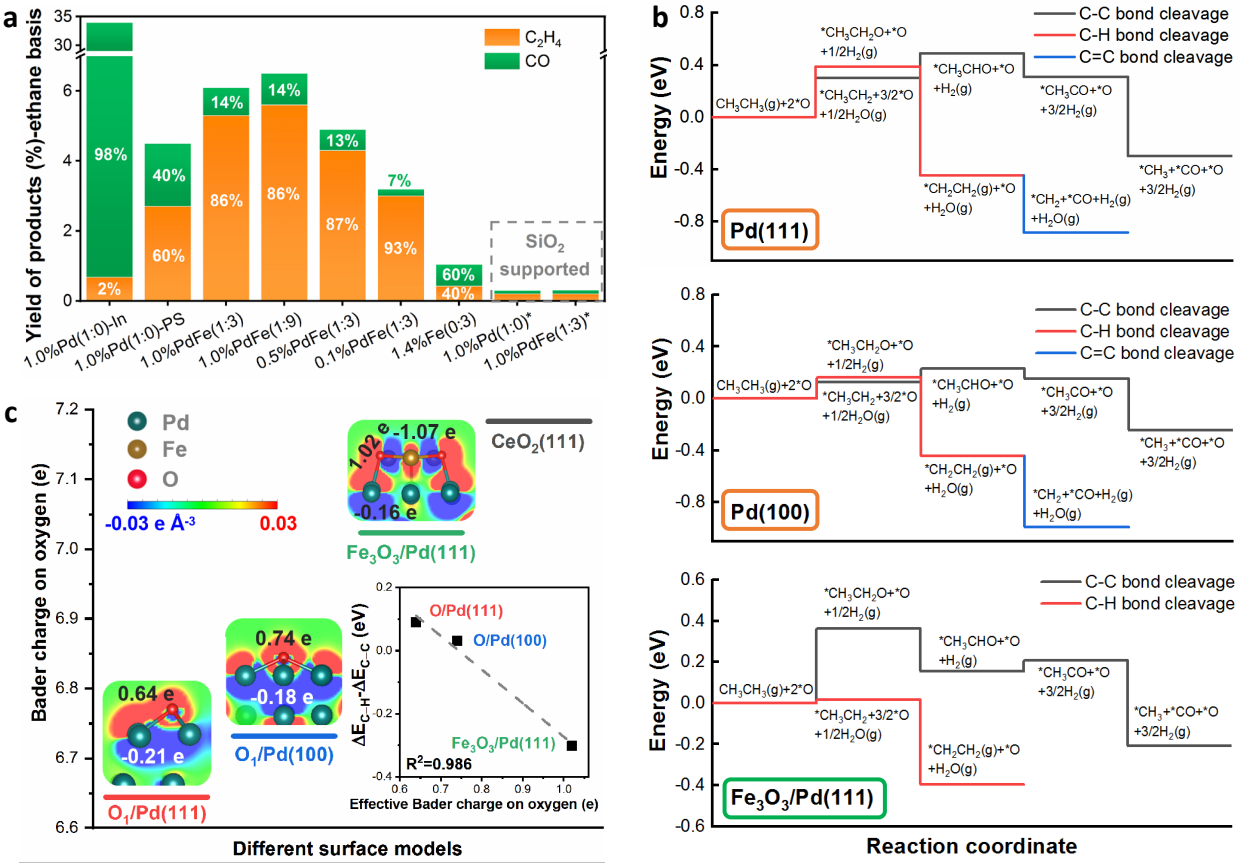

Figure 5. Correlation of selective bond cleavage of ethane with electronic properties of oxygen species. (a) Trend of C_2H_4 and CO yields over different catalysts. (b) Energy profiles of different reaction pathways on the Pd(111) , Pd(100), and Fe_3O_3/Pd(111) models. (c) Bader charge analysis of oxygen and contours of charge density on different configurations. The inset graph illustrates the correlation between the effective Bader charge on oxygen and the difference in the

reaction energy ($\Delta E_{C-H}-\Delta E_{C-C}$) of the selective C–H/C–C bond cleavage. Adapted with permission from ref. 3. Copyright 2020, Elsevier.

As a p-block element, In processes a lower ε_{coh} (243 vs 376 kJ/mol) and a larger $r_{W\text{-}S}$ (1.84 vs 1.52 Å) than Pd; moreover, In shows a lower work function (4.09 vs 5.41 eV) and electronegativity (1.78 vs 2.2), further emphasizing its oxophilic nature. Consequently, the PdIn system represents an extreme case of the segregation of the oxophilic element to the metal surface during the CO_2-ethane reaction. Through comprehensive characterization (Figure 6) involving in situ XRD, in situ XAS, AP-XPS, and STEM imaging, thin layers of InO_x were identified on the Pd(In) metal surface, leading to the formation of an InO_x/Pd interface within the PdIn/CeO_2 catalyst. This interface facilitated high C_2H_4 selectivity (>90%) and maintained stable conversion over a period of 110 hours with no observable coke deposition as indicated by both thermogravimetric analysis (TGA) and Raman spectroscopy. Notably, unlike the PdFe system, the oxygen species within the InO_x/Pd interface did not directly participate in C–H bond activation. Instead, the DFT calculations indicated that larger InO_x moiety weakened the adsorption of C_2H_xO* species (precursors for further C–C bond scission) but facilitated the desorption of C_2H_4, due to steric effects.[4] The presence of refined and ordered InO_x layers, attributed to the larger oxygen affinity of In than Fe, further distinguished it from its amorphous FeO_x counterparts.

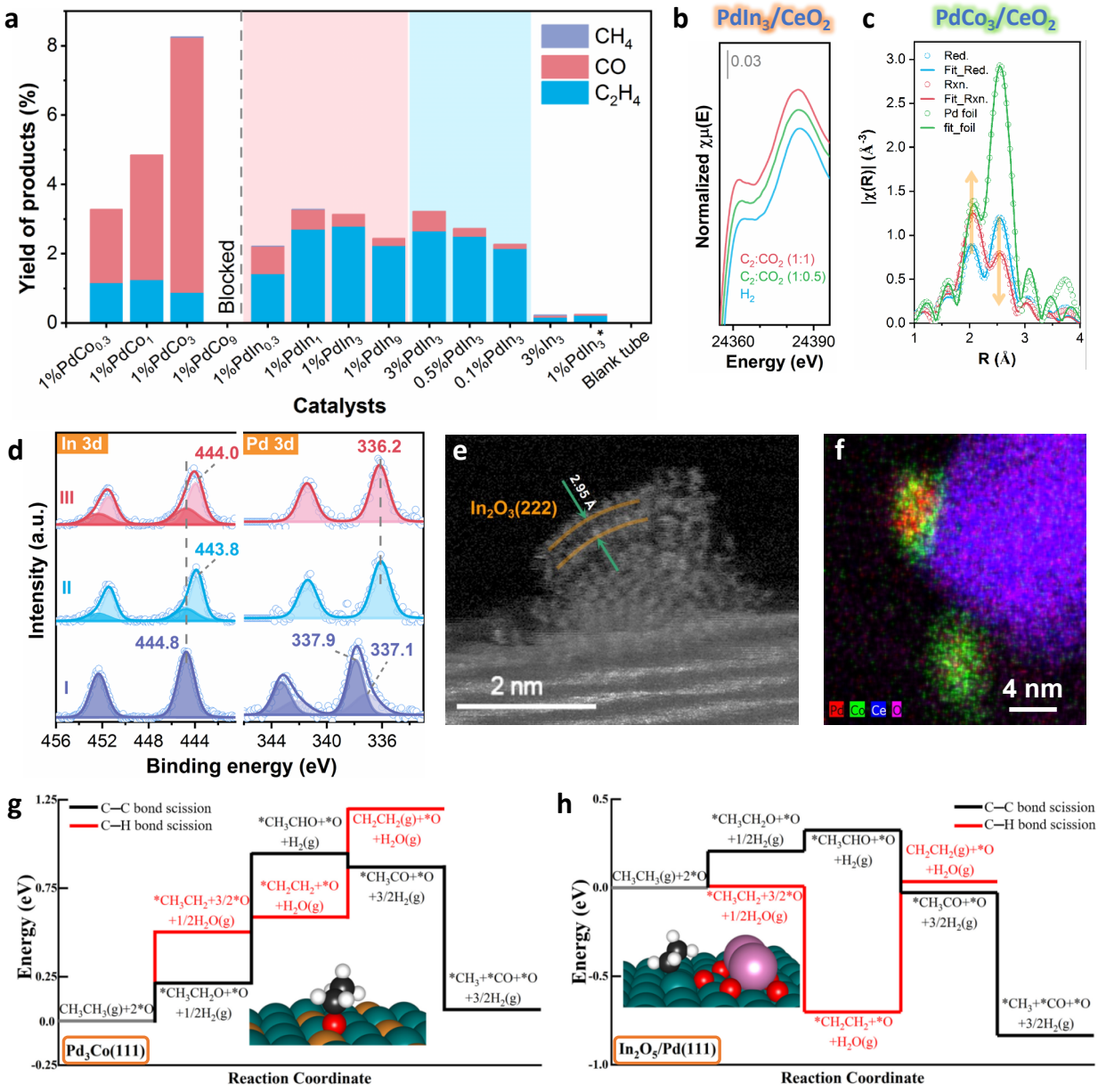

Figure 6. Effects of alloying and metal oxide/metal inverse interface on selective CO_2-ethane upgrading. (a) Product yields over $PdCo_x/CeO_2$ and $PdIn_x/CeO_2$ catalysts. (b) In situ Pd K-edge XANES spectra over $PdIn_3/CeO_2$ under various atmospheres. (c) In situ Pd K-edge FT-EXAFS spectra and fitting plots over $PdCo_3/CeO_2$ under the reduction and reaction conditions. (d) AP-XPS spectra of In 3d and Pd 3d core-levels over $PdIn_3/CeO_2$ under different conditions. (e) and (f) Electron microscopy over the spent $PdIn_3/CeO_2$ (e) and $PdCo_3/CeO_2$ (f) catalysts. (g) and (h) DFT-

calculated energetic profiles of reaction pathways over $Pd_3Co(111)$ (g) and $In_2O_5/Pd(111)$ (h) models. Adapted with permission from ref. 4. Copyright 2022, American Chemical Society.

3.4. Strong alloying effect in achieving metallic alloy structures

As a rule of thumb, the formation of alloy structure requires the relative cohesive energy less than 20% and/or the relative Wigner-Seitz radius less than 4% between the constituent elements. Like the PdFe case, Pd in the PdCo system[4] likely prefers to reside on the surface after reduction, while the oxygen-induced segregation potential of Co under reaction condition is lower than Fe in the PdFe system due to the larger work function (5.00 eV) and electronegativity (1.88) of Co. Thus, the PdCo alloy structure is expected to be retained under CO_2-ethane reaction conditions. The Pd 3d AP-XPS spectra and Pd K-edge XANES spectra indicated a metallic feature of the $PdCo_x/CeO_2$ catalysts (x = 1 or 3) under both the H_2-reduction and reaction conditions. The EXAFS spectra (Figure 6) indicated a greater extent of alloying under reaction conditions than that after reduction, as implied by the increased and decreased coordination numbers (CN) of Pd−Co and Pd−Pd bonds, respectively. The nearly identical CN of total Pd−M bonds suggested minimal metal agglomeration during the reaction. The in situ Co K-edge XANES spectra indicated a metallic feature similar to that of Co foil and Pd_xCo_y alloy. The in situ XRD analysis revealed the coexistence of Pd-rich PdCo alloy (dominated by Pd_3Co) and Co (hcp)-like phases, consistent with the HAADF-STEM imaging and EDS mapping. Given the low conversion of CO_2 and ethane of the control Co/CeO_2 catalyst, the fcc Pd_3Co phase was identified as the dominant active component. DFT calculations on the $Pd_3Co(111)$ surface indicated that, with the presence of O*, the CH_3CH_2* intermediate after the initial dissociation of ethane prefers to be oxidized to CH_3CH_2O*, followed by subsequent dehydrogenations and C-C bond cleavage to syngas, rather than dehydrogenation to $*CH_2CH_2$.

Likewise, the Pt-terminated PtNi alloy surface over a $PtNi/CeO_2$ catalyst was also identified to be favorable for the reforming pathway to produce syngas.[49] Pt exhibits strong backdonation capabilities from occupied metal d-orbitals to unoccupied antibonding C–H σ*-orbitals, enhancing C–H bond activation. Furthermore, Pt shows a notable affinity for p-block elements like Sn and In due to strong p-d orbital hybridization, often resulting in the formation of ordered intermetallic structures with robust heteroatomic bonding. These structures resist oxidation-induced segregation and enhance catalytic performance through strain, ligand, and ensemble effects. For these reasons, a $PtSn_3/\gamma\text{-}Al_2O_3$ catalyst[47] was evaluated for the CO_2-assisted ethane activation. In situ XAS experiments suggested a dominant Pt(Sn) clusters/SnO_x interfacial structures. Experimental and DFT results showed that this structure enabled simultaneous DHE (major), ODHE (minor), and DRE reactions, producing a mixture of $C_2H_4/CO/H_2$ with various ratios (e.g., 1.0/0.9/0.4), which can be fed to a downstream reactor for hydroformylation reaction[50] to produce C3 oxygenates. Notably, achieving the desired feed ratios (e.g., 1/1/1) for hydroformylation requires that catalysts should not solely favor oxidative dehydrogenation or reforming, setting additional demands for tuning selectivity.

3.5. General descriptors dictating thermodynamically favorable bimetallic-derived structures

While the factors mentioned above provide qualitative insights, quantitative understanding of thermodynamically stable structures under different conditions is lacking. Oxygen species from CO_2 dissociation has been identified to be crucial in selectively activating C–H/C–C bonds. However, understanding how the oxygen binding strength to bimetallic catalysts influences the catalyst structure preference and selective C–H/C–C bond cleavage remains limited. Nonetheless, the discussion above suggests that structural changes in bimetallic-derived catalysts primarily depend on the competition between alloying and surface segregation induced by oxidation.

As shown in Figure 7 and Table S1, based on a series of Pd-based bimetallic-derived catalysts (PdM, M=Ga, Sn, Fe, Ag, Au, Cu, Ni, Pt, Rh, Ru, and Ir),[4] two key factors have been identified as descriptors for controlling the selectivity of CO_2-assisted ethane activation: the formation energy of PdM_x surfaces and their reactive binding energy to oxygen. Unlike typical O* binding energy, the reactive O* binding energy accounts for the extra energy penalty or gain due to structural transformations (e.g., from mixed alloy to the skin or sandwich alloy) caused by O* adsorption. Generally, to achieve high selectivity towards C–H bond cleavage, a catalyst should have a strong O* binding to surpass the thermodynamic preference for alloy surface formation and drive the segregation of M as MO_x onto the surface. Conversely, when insufficient oxygen-induced driving force causes the alloy surface to remain stable under reaction conditions, preferential C–C bond cleavage occurs, resulting in CO and H_2 production. A comparative investigation utilizing In-based bimetallic-derived catalysts (MIn, M=Pt, Ni, Cu, Co, Rh, and Pd, see Table S1) further validated the general correlation.[51] Bimetallic-derived catalysts with high C_2H_4 selectivity should exhibit strong oxygen binding, facilitating the formation of oxide/metal interfaces under reaction

conditions. This favors ODHE over DRE by promoting stronger binding of the C_2H_x* species compared to C_2H_xO*, while still allowing for facile desorption of C_2H_4*. The trends and descriptors uncovered in these studies provide design principles for catalysts aimed at controlling selectivity in the simultaneous upgrading of CO_2 and ethane.

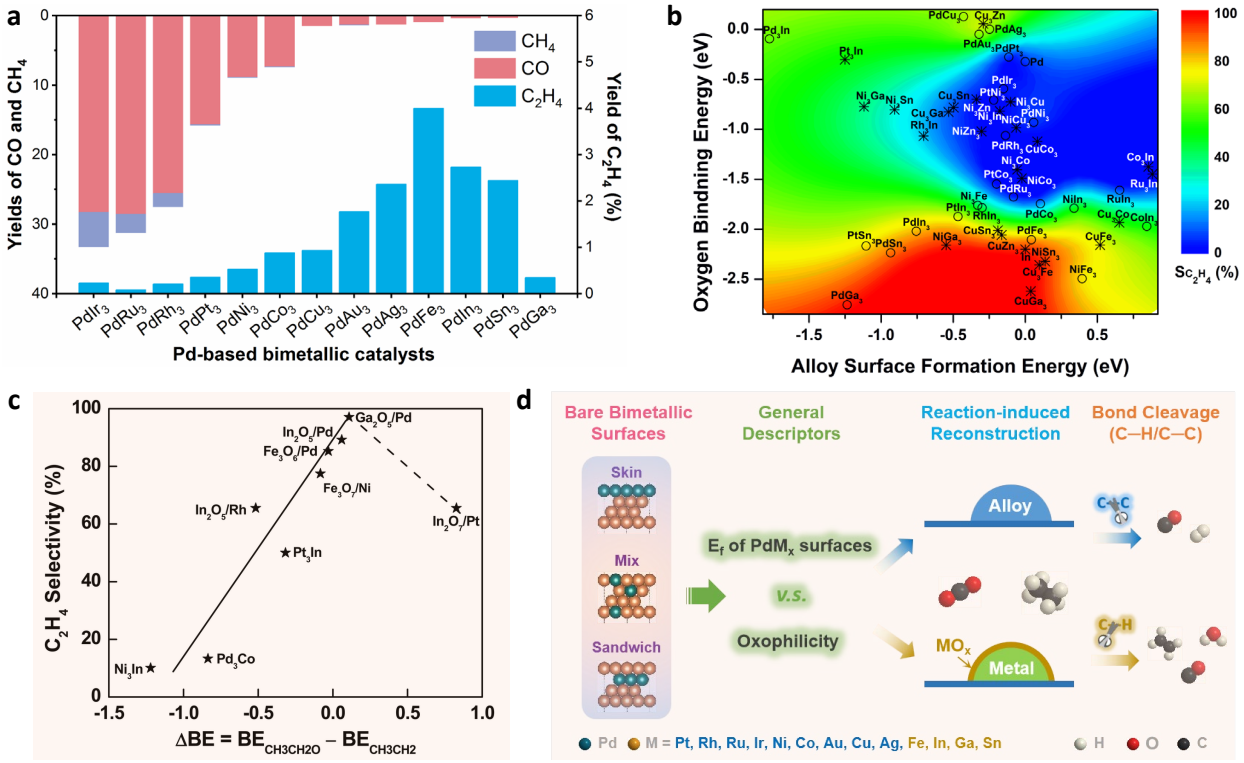

Figure 7. General descriptors depicting selective CO_2-ethane upgrading using various bimetallic-derived catalysts. (a) Trend of product yields over different PdM_3/CeO_2 catalysts. (b) Contour map for key descriptors: formation energy of PdM_3 slab and reactive *O binding energy on PdM_3, correlated with the C_2H_4 selectivity obtained under similar ethane conversion. (c) Correlation between C_2H_4 selectivity and binding energy difference of key initial intermediates, i.e., CH_3CH_2O* and CH_3CH_2* for DRE (C–C bond scission) and ODHE (C–H bond scission), respectively. (d) Interplay of general descriptors: guiding bimetallic-derived alloy or inverse

interface and selective CO_2-ethane upgrading. Adapted with permissions from ref. 4 (Copyright 2022, American Chemical Society) and ref. 51 (Copyright 2023, The Royal Society of Chemistry).

4. SUMMARY AND FUTURE OPPORTUNITIES

In typical supported bimetallic catalysts, multiple interactions (metal-metal, metal-support, and bimetallic/support/interface-adsorbate) create a wide array of unique structures (e.g., alloy, metal/support interface, and the metal oxide/metal interface) under reaction conditions. The relative cohesive energy and atomic (or Wigner-Seitz) radius serve as initial indicators to predict the alloying extent, while the difference in work function, electronegativity, and oxygen binding strength approximate the preference of forming suboxides by oxidation-induced segregation. It is essential to modify support reducibility and introduce surface defects through metal-support interfacial engineering to facilitate CO_2 activation and oxygen supply for ethane activation. Electron-deficient oxygen on metal or alloy surfaces promotes non-selective bond scission to produce syngas, while electron-enriched oxygen at metal oxide/metal inverse interfaces enhances selective C–H bond cleavage to produce ethylene. Elemental composition, oxygen-induced segregation, and strong alloying can regulate preferences for the formation of alloy surfaces or metal oxide/metal interfaces. The formation energy of alloy surfaces and their reactive oxygen binding energy offer insights into reaction-induced surface configurations for controlling the C−C/C−H bond scission using bimetallic-derived catalysts. Although these two key descriptors can depict the trend of syngas/ethylene selectivity in the case studies presented here, other factors like support effects, ensemble size, and crystalline facets require further DFT efforts. These two descriptors can also serve as the initial input for machine-learning studies to predict more efficient and sustainable bimetallic catalysts.

In ethane activation, CO_2-generated reactive oxygen species play a direct or indirect role in C–H bond activation. In the CO_2-ethane reaction for ethylene production, most reported bimetallic-derived catalysts undergo a stoichiometric conversion involving oxygen-assisted ethane activation, whereas efficient catalysts enabling simultaneous DHE and RWGS reactions are limited. Conventional DHE catalysts, such as PtSn-based catalysts, are facile to reach the equilibrium yield of olefins. Thus, exploring efficient RWGS coupling over these catalysts to break the non-oxidative dehydrogenation equilibrium yield holds promise for future advancements. Compared to CO_2-ODHE, DRE to syngas breaks the C–C bond into two carbon atoms, presenting higher carbon chemical potentials on the catalyst and increasing susceptibility to coke deactivation. Therefore, bimetallic catalysts that are effective for both ethane and CO_2 activation, weaken carbon binding strength, and provide sufficient (not excessive) electrophilic oxygen species are desired candidates for enhancing catalytic stability.

The emerging tandem-reactor strategy of producing oxygenates, involving in situ feeding the downstream hydroformylation reaction with the upstream CO_2-ethane reactions, presents further challenges in tuning the $C_2H_4/CO/H_2$ ratio. Conventional ODHE and DRE catalysts cannot meet this new requirement. Thus, it is necessary to explore new structure-function relationships and reaction mechanisms over bimetallic catalysts for simultaneous DHE+ODHE+RWGS or DHE+DRE+RWGS reactions. Additionally, integrating additional reaction chemistries (e.g., hydrocarboxylation: $C_2H_4+CO+H_2O \rightarrow CH_3CH_2COOH$) in the downstream reactor can expand value-added product types and improve atom efficiency from CO_2-ethane upgrading reactions. Crucially, verifying potential CO_2 reduction in the new tandem processes requires a comprehensive CO_2 footprint analysis.[16]

The intertwined nature of multiple interactions presents significant challenges in establishing structure-function correlations and can lead to structural heterogeneity, compromising catalytic performance. Hence, self-constrained and precise synthesis strategies (e.g., strong electrostatic adsorption, atomic layer deposition, galvanic replacement, and thermal shock methods) can be employed to potentially produce uniform alloy or inverse interfacial structures with optimized site densities. It is important to perform structural characterizations of these catalysts using a combination of time/spatial/energy-resolved in situ spectroscopy (e.g., XAS/AP-XPS/DRIFTS/Raman/EELS), scattering (e.g., electron/X-ray/neutron diffraction and total scattering), and microscopy (e.g., environmental TEM/STEM) techniques. Further coupling these comprehensive characterization techniques with online product analysis methods should enable the disentanglement of complex structural evolution under different conditions and facilitates the establishment of structure-function relationships in bimetallic-derived catalysts for CO_2-alkane reactions.

AUTHOR INFORMATION

Corresponding Author

* Jingguang G. Chen (jgchen@columbia.edu)

Author Contributions

Z.X. prepared the initial draft; Z.X. and J.G.C. reviewed and edited the manuscript. All authors have given approval to the final version of the manuscript.

Funding Sources

DE-SC0012704 from the US Department of Energy.

Notes

The authors declare no competing financial interest.

ACKNOWLEDGMENT

This work was financially supported by the Division of Chemical Sciences, Geosciences and Biosciences, Office of Basic Energy Sciences and carried out at Brookhaven National Laboratory, operated under contract DE-SC0012704 with the US Department of Energy.

Biographies

Dr. Zhenhua Xie is currently an Associate Research Scientist at the Department of Chemical Engineering at Columbia University and serving as a research staff in the Synchrotron Catalysis Consortium (SCC). His research interests lie on the simultaneous upgrading of carbon dioxide and shale gas into value-added chemicals by employing combined approaches of precise synthesis, kinetic analysis, in-situ synchrotron characterization, and theoretical calculations.

Dr. Jingguang Chen is the Thayer Lindsley Professor of Chemical Engineering at Columbia University, with a joint appointment at Brookhaven National Laboratory. His research interests include fundamental understanding of processes for carbon dioxide conversion. His research group utilizes combined approaches of experimental studies, in-situ characterization, and density functional theory calculations of thermocatalytic and electrocatalytic reactions.

REFERENCES

(1) Porosoff, M. D.; Myint, M. N. Z.; Kattel, S.; Xie, Z.; Gomez, E.; Liu, P.; Chen, J. G. Identifying Different Types of Catalysts for CO_2 Reduction by Ethane through Dry Reforming and Oxidative Dehydrogenation. *Angew. Chem. Int. Ed.* **2015**, *54*, 15501–15505.

(2) Yan, B.; Yao, S.; Kattel, S.; Wu, Q.; Xie, Z.; Gomez, E.; Liu, P.; Su, D.; Chen, J. G. Active Sites for Tandem Reactions of CO_2 Reduction and Ethane Dehydrogenation. *Proc. Natl. Acad. Sci. U.S.A.* **2018**, *115*, 8278–8283.

(3) Xie, Z.; Tian, D.; Xie, M.; Yang, S.-Z.; Xu, Y.; Rui, N.; Lee, J. H.; Senanayake, S. D.; Li, K.; Wang, H.; Kattel, S.; Chen, J. G. Interfacial Active Sites for CO_2 Assisted Selective Cleavage of C–C/C–H Bonds in Ethane. *Chem* **2020**, *6*, 2703–2716.

(4) Xie, Z.; Wang, X.; Chen, X.; Liu, P.; Chen, J. G. General Descriptors for CO_2-Assisted Selective C–H/C–C Bond Scission in Ethane. *J. Am. Chem. Soc.* **2022**, *144*, 4186–4195.

(5) Armstrong McKay, D. I.; Staal, A.; Abrams, J. F.; Winkelmann, R.; Sakschewski, B.; Loriani, S.; Fetzer, I.; Cornell, S. E.; Rockström, J.; Lenton, T. M. Exceeding 1.5°C Global Warming Could Trigger Multiple Climate Tipping Points. *Science* **2022**, *377*, eabn7950.

(6) Matthews, H. D.; Wynes, S. Current Global Efforts Are Insufficient to Limit Warming to 1.5°C. *Science* **2022**, *376*, 1404–1409.

(7) Chen, S.; Liu, J.; Zhang, Q.; Teng, F.; McLellan, B. C. A Critical Review on Deployment Planning and Risk Analysis of Carbon Capture, Utilization, and Storage (CCUS) toward Carbon Neutrality. *Renew. Sust. Energ. Rev.* **2022**, *167*, 112537.

(8) Biniek, K.; Henderson, K.; Rogers, M.; Santoni, G. Driving CO_2 Emissions to Zero (and beyond) with Carbon Capture, Use, and Storage. *McKinsey Quarterly* **2020**.

(9) Wang, D.; Xie, Z.; Porosoff, M. D.; Chen, J. G. Recent Advances in Carbon Dioxide Hydrogenation to Produce Olefins and Aromatics. *Chem* **2021**, *7*, 2277–2311.

(10) De Luna, P.; Hahn, C.; Higgins, D.; Jaffer, S. A.; Jaramillo, T. F.; Sargent, E. H. What Would It Take for Renewably Powered Electrosynthesis to Displace Petrochemical Processes? *Science* **2019**, *364*, eaav3506.

(11) Lin, H.; Luo, S.; Zhang, H.; Ye, J. Toward Solar-Driven Carbon Recycling. *Joule* **2022**, *6*, 294–314.

(12) Wang, Q.; Kalathil, S.; Pornrungroj, C.; Sahm, C. D.; Reisner, E. Bacteria–Photocatalyst Sheet for Sustainable Carbon Dioxide Utilization. *Nat. Catal.* **2022**, *5*, 633–641.

(13) Eiermann, J. U.S. Ethane Exports Set a Monthly Record in March 2023. June 12, 2023. https://www.eia.gov/todayinenergy/detail.php?id=56780.

(14) Xie, Z.; Winter, L. R.; Chen, J. G. Bimetallic-Derived Catalysts and Their Application in Simultaneous Upgrading of CO_2 and Ethane. *Matter* **2021**, *4*, 408–440.

(15) Xie, Z.; Gomez, E.; Chen, J. G. Simultaneously Upgrading CO_2 and Light Alkanes into Value-Added Products. *AIChE J.* **2021**, *67*.

(16) Biswas, A. N.; Winter, L. R.; Xie, Z.; Chen, J. G. Utilizing CO_2 as a Reactant for C_3 Oxygenate Production via Tandem Reactions. *JACS Au* **2023**, *3*, 293–305.

(17) Biswas, A. N.; Xie, Z.; Chen, J. G. Can CO_2-Assisted Alkane Dehydrogenation Lead to Negative CO_2 Emissions? *Joule* **2022**, *6*, 269–273.

(18) Yu, W.; Porosoff, M. D.; Chen, J. G. Review of Pt-Based Bimetallic Catalysis: From Model Surfaces to Supported Catalysts. *Chem. Rev.* **2012**, *112*, 5780–5817.

(19) Liu, L.; Corma, A. Bimetallic Sites for Catalysis: From Binuclear Metal Sites to Bimetallic Nanoclusters and Nanoparticles. *Chem. Rev.* **2023**, *123*, 4855–4933.

(20) B1: Workfunction Values (Reference Table). https://chem.libretexts.org/Ancillary_Materials/Reference/Reference_Tables/Bulk_Properties/B1%3A_Workfunction_Values_(Reference_Table). Accessed at June 2023.

(21) Helmenstine, A. *Electronegativity Definition and Trend*. https://sciencenotes.org/electronegativity-definition-and-trend/. Accessed at June 2023.

(22) Kittel, C.; McEuen, P. *Introduction to Solid State Physics*; John Wiley & Sons, 2018.

(23) Yan, Y.; Du, J. S.; Gilroy, K. D.; Yang, D.; Xia, Y.; Zhang, H. Intermetallic Nanocrystals: Syntheses and Catalytic Applications. *Adv. Mater.* **2017**, *29*, 1605997.

(24) Eom, N.; Messing, M. E.; Johansson, J.; Deppert, K. General Trends in Core–Shell Preferences for Bimetallic Nanoparticles. *ACS Nano* **2021**, *15*, 8883–8895.

(25) Wang, L.-L.; Johnson, D. D. Predicted Trends of Core−Shell Preferences for 132 Late Transition-Metal Binary-Alloy Nanoparticles. *J. Am. Chem. Soc.* **2009**, *131*, 14023–14029.

(26) Li, Y.; Zhang, Y.; Qian, K.; Huang, W. Metal–Support Interactions in Metal/Oxide Catalysts and Oxide–Metal Interactions in Oxide/Metal Inverse Catalysts. *ACS Catal.* **2022**, *12*, 1268–1287.

(27) Van Deelen, T. W.; Hernández Mejía, C.; De Jong, K. P. Control of Metal-Support Interactions in Heterogeneous Catalysts to Enhance Activity and Selectivity. *Nat. Catal.* **2019**, *2*, 955–970.

(28) Ernst, F. Metal-Oxide Interfaces. *Mater. Sci. Eng. R Rep.* **1995**, *14*, 97–156.

(29) Luo, Z.; Zhao, G.; Pan, H.; Sun, W. Strong Metal–Support Interaction in Heterogeneous Catalysts. *Adv. Energy Mater.* **2022**, *12*, 2201395.

(30) Etim, U. J.; Zhang, C.; Zhong, Z. Impacts of the Catalyst Structures on CO_2 Activation on Catalyst Surfaces. *Nanomaterials* **2021**, *11*, 3265.

(31) Álvarez, A.; Borges, M.; Corral-Pérez, J. J.; Olcina, J. G.; Hu, L.; Cornu, D.; Huang, R.; Stoian, D.; Urakawa, A. CO_2 Activation over Catalytic Surfaces. *ChemPhysChem* **2017**, *18*, 3135–3141.

(32) Menning, C. A.; Chen, J. G. General Trend for Adsorbate-Induced Segregation of Subsurface Metal Atoms in Bimetallic Surfaces. *J. Chem. Phys.* **2009**, *130*, 174709.

(33) Moltved, K. A.; Kepp, K. P. The Chemical Bond between Transition Metals and Oxygen: Electronegativity, d-Orbital Effects, and Oxophilicity as Descriptors of Metal–Oxygen Interactions. *J. Phys. Chem. C* **2019**, *123*, 18432–18444.

(34) Ward, A. F. H.; Bharucha, N. R. The Relationship between the Work Function of a Metal and Its Energy of Activation for Oxidation. *Recl. Trav. Chim. Pays-Bas* **1953**, *72*, 735–738.

(35) Rodriguez, J. A.; Liu, P.; Graciani, J.; Senanayake, S. D.; Grinter, D. C.; Stacchiola, D.; Hrbek, J.; Fernández-Sanz, J. Inverse Oxide/Metal Catalysts in Fundamental Studies and Practical Applications: A Perspective of Recent Developments. *J. Phys. Chem. Lett.* **2016**, *7*, 2627–2639.

(36) Xie, Z.; Hwang, S.; Chen, J. G. Reduction-induced Metal/Oxide Interfacial Sites for Selective CO_2 Hydrogenation. *SmartMat* **2023**, e1201.

(37) Ruiz Puigdollers, A.; Schlexer, P.; Tosoni, S.; Pacchioni, G. Increasing Oxide Reducibility: The Role of Metal/Oxide Interfaces in the Formation of Oxygen Vacancies. *ACS Catal.* **2017**, *7*, 6493–6513.

(38) Xie, Z.; Yan, B.; Kattel, S.; Lee, J. H.; Yao, S.; Wu, Q.; Rui, N.; Gomez, E.; Liu, Z.; Xu, W.; Zhang, L.; Chen, J. G. Dry Reforming of Methane over CeO_2-Supported Pt-Co Catalysts with Enhanced Activity. *Appl Catal B-Environ.* **2018**, *236*, 280–293.

(39) Xie, Z.; Yan, B.; Lee, J. H.; Wu, Q.; Li, X.; Zhao, B.; Su, D.; Zhang, L.; Chen, J. G. Effects of Oxide Supports on the CO_2 Reforming of Ethane over Pt-Ni Bimetallic Catalysts. *Appl Catal B-Environ.* **2019**, *245*, 376–388.

(40) Xiong, M.; Gao, Z.; Qin, Y. Spillover in Heterogeneous Catalysis: New Insights and Opportunities. *ACS Catal.* **2021**, *11*, 3159–3172.

(41) Yao, R.; Herrera, J. E.; Chen, L.; Chin, Y.-H. C. Generalized Mechanistic Framework for Ethane Dehydrogenation and Oxidative Dehydrogenation on Molybdenum Oxide Catalysts. *ACS Catal.* **2020**, *10*, 6952–6968.

(42) Yao, R.; Pinals, J.; Dorakhan, R.; Herrera, J. E.; Zhang, M.; Deshlahra, P.; Chin, Y.-H. C. Cobalt-Molybdenum Oxides for Effective Coupling of Ethane Activation and Carbon Dioxide Reduction Catalysis. *ACS Catal.* **2022**, *12*, 12227–12245.

(43) Zhai, P.; Xie, Z.; Huang, E.; Aireddy, D. R.; Yu, H.; Cullen, D. A.; Liu, P.; Chen, J. G.; Ding, K. CO_2-Mediated Oxidative Dehydrogenation of Propane Enabled by Pt-Based Bimetallic Catalysts. *Chem* **2023**, https://doi.org/10.1016/j.chempr.2023.07.002.

(44) Becke, A. D. Tracking C–H Activation with Orbital Resolution. Science **2023**, *380*, 955-960.

(45) Crabtree, R. H. *The Organometallic Chemistry of the Transition Metals*; John Wiley & Sons, **2009**.

(46) Balcells, D.; Clot, E.; Eisenstein, O. C—H Bond Activation in Transition Metal Species from a Computational Perspective. *Chem. Rev.* **2010**, *110*, 749–823.

(47) Xie, Z.; Guo, H.; Huang, E.; Mao, Z.; Chen, X.; Liu, P.; Chen, J. G. Catalytic Tandem CO_2 –Ethane Reactions and Hydroformylation for C3 Oxygenate Production. *ACS Catal.* **2022**, *12*, 8279–8290.

(48) Najari, S.; Saeidi, S.; Concepcion, P.; Dionysiou, D. D.; Bhargava, S. K.; Lee, A. F.; Wilson, K. Oxidative Dehydrogenation of Ethane: Catalytic and Mechanistic Aspects and Future Trends. *Chem. Soc. Rev.* **2021**, *50*, 4564–4605.

(49) Yan, B.; Yang, X.; Yao, S.; Wan, J.; Myint, M.; Gomez, E.; Xie, Z.; Kattel, S.; Xu, W.; Chen, J. G. Dry Reforming of Ethane and Butane with CO_2 over $PtNi/CeO_2$ Bimetallic Catalysts. *Acs Catalysis* **2016**, *6*, 7283–7292.

(50) Xie, Z.; Xu, Y.; Xie, M.; Chen, X.; Lee, J. H.; Stavitski, E.; Kattel, S.; Chen, J. G. Reactions of CO_2 and Ethane Enable CO Bond Insertion for Production of C3 Oxygenates. *Nature Communications* **2020**, *11*, 1887.

(51) Guo, H.; Xie, Z.; Wang, X.; Chen, J. G.; Liu, P. Descriptor-Based Identification of Bimetallic-Derived Catalysts for Selective Activation of Ethane with CO_2. *EES. Catal.* **2023**, *1*, 17–25.
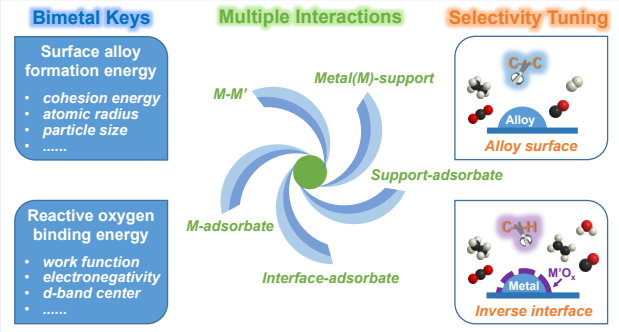
Conspectus Graphic